Wireless Power Transfer System For Electric Vehicle Charging

Pedro Lopes
Instituto Superior Técnico de Lisboa
University of Lisbon
Lisboa, Portugal
pedro.conceicao.lopes@tecnico.ulisboa.pt

Sónia Pinto
Instituto Superior Técnico de Lisboa
University of Lisbon
Lisboa, Portugal
soniafp@tecnico.ulisboa.pt

Pedro Costa
Instituto Superior Técnico de Lisboa
University of Lisbon
Lisboa, Portugal
pedro.b.costa@tecnico.ulisboa.pt

***Abstract*-The research regarding new ways of charging an electric vehicle (EV) is a treading research topic. Wireless charging is one of many technologies currently being investigated and preferred for various applications. With this technology, there is no physical connection between the EV and the charging station, providing a pleasant experience between the vehicle and the user. However, the question arises about how well it performs compared with other technologies of EV's. This thesis studied the behavior of a prototype of a wireless power transfer system for EVs that was designed and built to analyze and understand the wireless charging process. A first analysis was made on the operating principles of wireless power transfer supported on the state of the art of the currently used technologies. The resonant wireless charging was selected as the best candidate for the prototype model based on physical and power demands. Important concepts related to these technologies were mentioned, such as zero voltage and zero current switching and compensation networks. A 100 W inductive charger prototype using a resonant tank was designed and tested using the Simulink and Matlab software. A controller was dimensioned and simulated to control the load voltage. A prototype was built to scale, and experimental tests were carried out to validate the proposed topology and controller. The experiment data was analyzed, and conclusions were drawn regarding the resonant inductive charger's overall performance.**

Keywords-Wireless Charging, Power Transfer, Compensation network, Resonant Tank

Introduction

The need for sustainable means of transportation, caused by the depletion of fossil fuels, has led to the growth in the research and innovation of EV technologies. According to 2020 Global EV Outlook [1], an annual publication that identifies and discusses recent electric mobility developments worldwide, EVs' sales continue to rise. In 2019, 2.1 million were sold, surpassing 2018, registering a 40% year-on-year increase, which leads to the assumption that EV's are a solution to continue to grow over the following years. A global EV forecast [2] predicts a total EV sales growing from 2.5 million in 2020 to 11.2 million in 2025, then reaching 31.1 million by 2030.

Carbon emissions pose severe challenges for the sustainability of future generations. Part of this risk is due to the transportation industry [3]. According to the Health World Organization, transportation accounted for about 23% of global carbon dioxide emissions in 2010 and 27% of end-use energy emissions, with urban transport accounting for about 40% of end-use energy consumption [4].

One solution to lower the carbon dioxide emissions caused by the urban transportation sector is to replace fossil-based fuels with green sources such as electrical energy [5]. Vehicles that use electrical energy as their primary source of power are the so-called electrical vehicles (EV). An EV can be categorized broadly into Battery electric vehicle (BEV), which runs solely on electricity and the hybrid electric vehicle (HEV) that combines the electric energy with other sources of renewable energy or in many cases they have a standard internal combustion engine that runs in fossil-fuel [6]. Nowadays, these vehicles mainly use Li-Ion batteries [7].

Wireless charging consists of transferring energy from the source to the load without the need for any wires. WPT is not new, as Nikola Tesla had patented WPT over 100 years ago [8]. Nowadays, WPT systems are used both on short and long-range applications. There are some examples of electric toothbrushes on short-range applications that use inductive charging and, more recently, smartphone chargers. The WPT systems used on EV's are considered long-range applications.

Besides this classification of long and short-range, wireless charging systems (WCS) can be used in a static mode where the battery is charged when the vehicle is parked, or in a dynamic model where the battery is being charged is in motion [9]. This thesis focuses on stationary WCS.

The large majority of the WPT systems are inductive power transfer (IPT) systems. According to [10], IPT systems are defined as systems where energy is transferred from a primary winding to a secondary using a magnetic field. Such systems can be divided into two categories: 1) closely coupled IPT systems and 2) loosely coupled IPT systems. In closely coupled IPT systems, the magnetic coupling between the primary and the secondary side is perfect, i.e., the leakage inductance is small compared to the magnetizing inductance in the system. The second system is the opposite: the magnetic coupling between both sides is low, and the leakage inductance is usually much higher than the magnetizing inductance of the system, resulting in low efficiency of the charging process..

The following objectives of all the research being done on this topic are as follow: Review on the background and state-of-art of WPTS; Establish the link between the thesis topic and the state-of-art; Design of a loosely coupled IPT system based on current WPT technologies to optimize the general efficiency of the process; To design a simulation model of an inductive charger; Design a control system to command the semiconductors; Design and build an experimental prototype to validate both the designed controller and the selected topology; Provide results and documentation for the future development of this technology.

I. Background and State-Of-Art

A. Basic Concept of Wireless Power Transfer

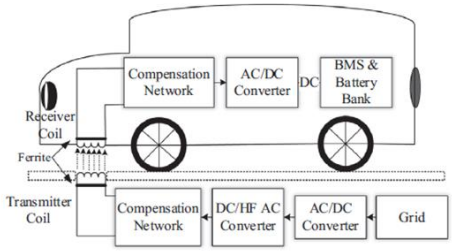

Figure 1-Basic block diagram of WPT (Courtesy of Panchal et al.).

The standard block diagram of a WPT system used for an Electric Vehicle (EV) is illustrated in Figure 1 [9]. In this early stage of the work, let this generic block diagram represent an IPT system as used in most WPTS. Even though the figure shows the power transferred by two coils, there are many possible configurations for the coil system. In some cases, it is used more than two coils like four-coil structures [11], and also the shape and size of the coils play a crucial role in the efficiency of the WPT, but since the scope of this work is not focused on the physical geometry and properties of the coils system it is now going to be further developed. The charging process is comprised of 3 essential parts: The transmitting and receiving coils. These coils may assume different shapes and types of materials that influence the charging process's overall efficiency, as it is going to be shown in later sections; the compensation networks; the power electronics converters.

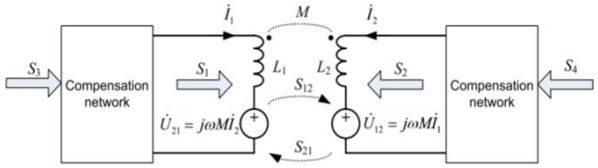

Figure 2-Two-coil WPT system (Courtesy of S.Li et al.).

By looking at Figure 2, it is possible to identify L_1 which is the self-inductance of the primary side or transmitting coil and L_2 represents the self-inductance of the secondary side or receiving coil. $\dot{I}_1$and $\dot{I}_2$ are the currents in the two coils, $\dot{U}_{12}$ is the voltage in the secondary coil that is induced by the current in the primary side, $\dot{U}_{21}$ is the voltage in the primary coil induced by the secondary coil current due to coupling or mutual inductance between the primary and secondary coils. S_1 and S_2 are the apparent power provided by the power converter. $\dot{S}_{12}$ and $\dot{S}_{21}$represent the apparent power exchanged between the two coils. For this analysis, the coil resistance and magnetic losses are neglected and, from L_1 and L_2, it is possible to formulate the equations of the exchanged complex power: $\dot{S}_{12}$ (1) and $\dot{S}_{21}$ (2), where I_1 and I_2 are the roots, mean square values of the currents and φ_{12} is the phase difference between $\dot{I}_1$ and $\dot{I}_2$.

$$\dot{S}_{12} = -\dot{U}_{12}\dot{I}^*_2 = -j\omega M\dot{I}_1\dot{I}^*_2 = \\ = \omega M I_1 I_2 \sin\varphi_{12} - j\omega M I_1 I_2 \cos\varphi_{12} \quad (1)$$

$$\dot{S}_{12} = -\dot{U}_{12}\dot{I}^*_2 = -j\omega M\dot{I}_1\dot{I}^*_2 = \\ = \omega M I_1 I_2 \sin\varphi_{12} - j\omega M I_1 I_2 \cos\varphi_{12} \quad (2)$$

From (1), the active power transfer from the primary side to the secondary can be maximized by assuring that the phase difference between both current, φ_{12} , is around 90 º as expressed:

$$P_{12} = \omega M I_1 I_2 \sin\varphi_{12} \quad (3)$$

Assuming $\varphi_{12} = \frac{\pi}{2}$, means that the total complex power that goes into the two-coil system is then given by:

$$\dot{S} = \dot{S}_1 + \dot{S}_2 = j\omega(L_1 I_1^{\,2} + L_2 I_2^{\,2} + 2M I_2 I_1 \cos\varphi_{12}) \quad (4)$$

Therefore, the reactive power *Q* that goes into the two-coil system is:

$$Q = \omega(L_1 I_1^{\,2} + L_2 I_2^{\,2} + 2M I_2 I_1 \cos\varphi_{12}) \quad (5)$$

From the fundamentals of traditional transformers, reactive power represents the magnetizing power. Thus, higher magnetizing power results in higher copper and core losses. When computing the efficiency of transformers, two essential parameters come to play. One is the coupling coefficient of the windings or the quality of the magnetic circuit usually expressed by *k*, and the other is the quality factor Q_L. The coupling coefficient appears in the expression of the mutual inductance *M:*

:

$$M = k\sqrt{L_1 L_2} \quad (6)$$

The coupling coefficient *k* ranges from 0 to 1, where 1 means that all the magnetic flux produced from one coil passes through the other coupled coil, and so the efficiency becomes higher. The inductor quality factor Q_L is given by the ratio between the inductor reactance and its resistance at a given frequency:

$$Q_L = \frac{\omega_L}{R_L} \quad (7)$$

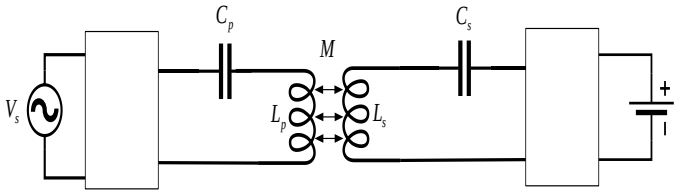

Figure 3-Resonant inductive charger.

Some new WPT methods appeared in the last years using this principle described inductive power transfer, such as capacitive, permanent magnet, and resonant inductive charging, which is the most popular WPT technology *[12]*. This technique uses two or more tuned resonant tanks, based on LC circuits, resonating at the same frequency. A typical example is shown in Figure 3, where both sides of the charger have a capacitor and an inductance.

Using resonant circuits bring many advantages compared to the regular inductive charging that only used the two coils

system, such as: Maximizing the transferred power; Optimizing the transmission efficiency; Controlling the transmitted power by frequency variation; Creating a specific source characteristic (current or voltage source); Compensating variation of the magnetic coupling; Compensating the magnetizing current in the transmitter coil to reduce generator losses; Matching the transmitter coil impedance to the generator; Suppressing higher harmonics form the generator.

B. *Zero Voltage Switching (ZVS) and Zero Current Switching (ZCS)*

WPT systems require power converters such as rectifiers and inverters, to enable the charging process. The topologies used for the power converters require semiconductors such as MOSFET's, IGBT's, Diodes or, at higher switching frequencies, wide bandgap semiconductors as SiC (Silicon Carbide) MOSFETs or GaN HEMTs (Gallium Nitride, High Electron Mobility Transistors). Power switches have to turn-on and turn-off depending on if it is required or not to feed the load under hard-switching conditions. Hard switching refers to the stressful switching behavior of the power electronic devices [13]. The switching trajectory of a hard-switched power device can be seen in Figure 4.

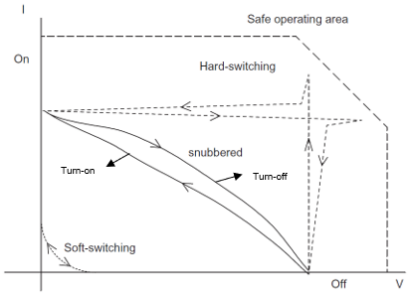

Figure 4-Typical switching trajectories of power switches (Courtesy of M.H.Rashid et al.).

During this hard switching, the power device has to withstand high voltage and current, resulting in high switching losses and stress. It is possible to have dissipative elements to reduce these switching losses, as shown in Figure 4, where a snubber circuit (consisting of passive elements) is used to dissipate some of the energy resulting from the hard switching. However, this approach results in switching power losses from the switch to the snubber, and as a result, the overall efficiency decreases. There is another factor to be considered that is the power devices switching frequency. The higher the switching frequency, the higher the switching losses.

To overcome this problem regarding the switching losses, resonant converters are used. Resonant converter as the name infers, includes a resonant tank, with LC circuit operating at resonance frequency, to create oscillatory voltage and/or current waveforms so that ZVS and ZCS conditions occur. This resonant tank is also used to store, and transfer energy from the input to the output in a manner similar to the conventional resonant converter [14].

The ZCS operation consists of shaping the device's currents using the resonant tank at on-time to create zero-current conditions for the device to turn off. In ZVS the voltage waveform is shaped so that at the off-time the device is in zero-voltage conditions to the device to turn on.

C. *Compensation Topologies*

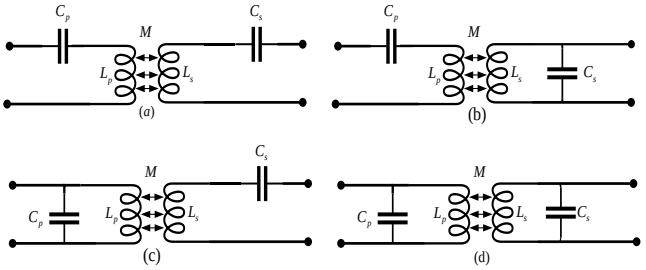

Figure 5-Compensation Topology (a) Series-Series (b) Series-Parallel (c) Parallel-Series (d) Parallel-Parallel.

As shown in Figure 5 [15], capacitors introduction on the primary and secondary sides are essential to eliminate the phase difference between current and voltage and minimize the reactive power in the power source. The compensation network is also responsible for tuning the circuit to have the same resonance frequency as the transmitter to maximize the power transfer. Other benefits of using compensation networks are the help they give to have a soft switching of power transistors, reduce switching losses, and have constant current and constant voltage charging [15] . It is fair then to assume that even though having more elements implies having a more complex topology. It is essential to have a compensation network when designing a WPTS since it benefits the charging process. The four main types of compensation network topologies are shown in figure 5:Series-Series (SS), Series-Parallel (SP), Parallel-Series (PS), and Parallel-Parallel (PP).

Although each of the four topologies has its pros and cons, the most used topology in EV is the SS because of two significant advantages [9]. On the SS-compensated topology, the value of the capacitor in the source and receiving sides does not influence the mutual inductance and does not affect the load conditions, and so the resonant frequencies of the source and receiver sides depend only on the self-inductance of the primary and secondary coils [16] [17]. The other advantage is that the power factor is maintained near one, and so higher efficiencies can be obtained for this compensation topology.

To achieve soft-switching in power electronic converts, the primary side of the compensation network is often tuned to make the primary reach zero voltage switching (ZVS) or zero current switching (ZCS) condition [18].

The series and/or parallel configurations are added to both sides to create the resonant conditions achieved when the energy stored in the capacitor equals the energy stored in the inductor, i.e., when both components have the same impedance [19].To obtain the value of the resonant angular frequency ω_0 is obtained by equaling the inductor impedance to the capacitor impedance of the resonant tank:

$$\omega_0 L_{p,s} = \frac{1}{\omega_0 C_{p,s}} \Rightarrow \omega_0 = \frac{1}{\sqrt{L_{p,s} C_{p,s}}} \tag{8}$$

The linear resonant frequency f_r can also be expressed by the following expression:

$$f_{r(p,s)}=\frac{1}{2\pi\sqrt{L_{p,s}C_{p,s}}} \quad (9)$$

II. Simulation of an IPTS for EV charger

This section presents a single-phase computational IPT model, illustrated in appendix A, to simulate a generic load's charging process dynamically. A flowchart is presented in Figure 6 with the steps that were followed when designing this prototype.

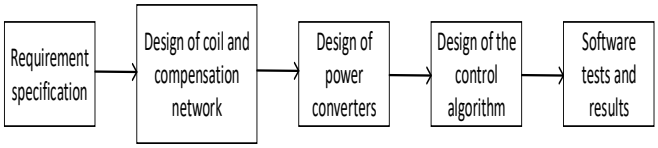

Figure 6-Flowchart for the design of the IPT charger.

The main goal is to prove the importance of having a compensation network to improve the inductive charger's general power transfer capability while using the principle of resonant inductive coupling.Based on the results, conclusions were drawn on the charging process performance. All simulations were made using the software Simulink and MATLAB [20]. Before designing the prototype, it is essential to define which of the main requirements for the IPT. The requirements specifications are as follow:The power transferred to the generic load of 100 W.;The supply grid will have the nominal 230 V and frequency of 50 Hz; Nominal voltage at the generic load is 15 V; Simple control algorithm; Capacity for bidirectional power flow if any V2G was to be used; The opted operational frequency for this application is 150 kHz.The final model of the charger is illustrated in Figure 7.

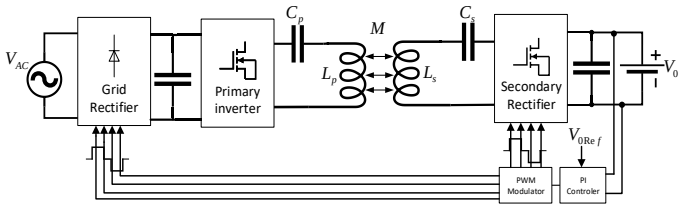

Figure 7-Topology of the wireless charger.

A. Design of the coils and Compensation Network

One of the leading causes of low efficiencies is the weak coupling due to the large leakage inductance in both sides of the IPT Transformer. A simplified equivalent circuit of the IPT is shown in Figure 8.

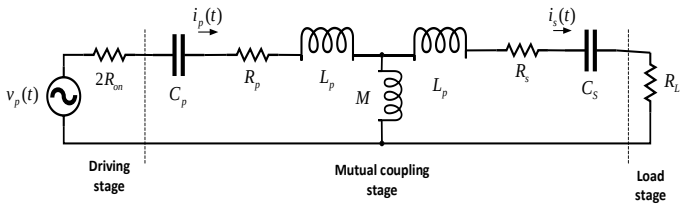

Figure 8-IPT equivalent circuit.

The equivalent model is divided into three parts. The driving stage represents the AC source, v_P, plus a conduction resistance, R_{ON}, of any converter that may appear before the IPT. The mutual coupling stage is modeled using a T-network. The resistance of the primary coil and secondary are represented by R_P and R_S. The resistance represents the load R_L. M is the mutual inductance between the two coils, which is related to k and the primary and secondary self-inductances L_P and L_S as it is shown in equation (6).

An inductance is associated with the uncoupled flux or leakage flux called leakage inductance on typical transformers [21] . The leakage inductances on the primary and secondary sides, L_{Pk} and L_{Sk} are expressed as a function of *k*:

$$\begin{aligned} L_{Pk} &= (1-k)L_P \\ L_{Sk} &= (1-k)L_S \end{aligned} \quad (10)$$

The primary and secondary resonant circuits are designed to resonate at the same frequency. The resonance frequency is given by (21). When the circuit is driven at the resonance frequency on both sides, the primary and secondary sides' leakage reactance is canceled out by the capacitive reactance. Thus, by introducing a compensative network with the capacitors C_P and C_S the overall efficiency of the charging process is expected to increase.

The process of designing the coils have a significant effect on the overall efficiency of the charging process. Factors such as the dimensions, weight, material, and the number of coils should be well analyzed. But since this simulation aims to prove the overall superior efficiency of using a compensation network, a 1:1 system of coils is used. The primary and secondary coil are the same with all the specifications given in the datasheet [22] supplied by Wurth Elektronik™.

Table 1-Properties of the wireless coil.

Property	$L_p(\mu H)$	$L_s(\mu H)$	$M(\mu H)$
Value	5.8	5.8	2.9

The properties of the wireless coil are defined in Table 1. The value of mutual inductance M is defined by the equation (6), considering the coupling factor, *k*, equal to 0.5.

The compensation network selected is the series-series topology since, as it was previously mentioned, it is the most popular of all the topologies mentioned before. The computation of the capacitors is derived from the equations (8) and (9) which by assuming that the tank composed of the compensation capacitor and the wireless inductor at each side of the charger, working at 0.9 of the operational frequency, $f_o = 135\ kHz$. The following expression can be deduced to arrive at the value of each capacitor:

$$C_p = \frac{1}{L_p\omega_0^{\,2}} = C_s = \frac{1}{L_s\omega_0^{\,2}} = 48nF \quad (11)$$

This being said, the resonant tank diagram used in the simulation is composed of a two winding linear transformer block with a turn ratio of 1:1. The winding resistances' values were 1 % of the total losses on the transformer and both windings have a series-series topology, i.e., the compensations capacitor are in series with the winding inductance.

B. Control Design

There are two power converters on this prototype design: a Voltage Source Converters (VSCs on the primary side and a Voltage Source Converters (VSCs on the secondary side. The primary converter is essential to control the amount of power transferred to the resonant tank. The secondary side's converter converts the AC signals coming from the resonant tank to a controlled DC voltage used to supply the load. A single-phase full bridge topology was used on both VSCs, with MOSFETs and diodes placed in parallel, as illustrated in Figure 9. The gate signals of each transistor are going to be generated at the operational frequency of 150 kHz and a control algorithm is going to be implemented so that it is possible to control the gate signals.

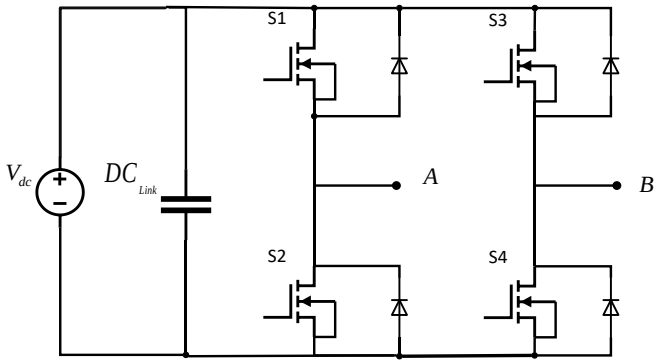

Figure 9-IGBT single phase VSC.

The control algorithm was implemented in the secondary converter to regulate the power transfer. The converter controller was designed so that the phase between the primary and secondary voltage waveforms ensures a specific load voltage through the charging process.

This controller measures the voltage being applied to the load to determine the phase shift and control the transistor switching to implement the phase shift.

Figure 10 shows the overall control scheme. The power converter is modeled with a gain, K_D, and a time delay, T_d . The voltage error is obtained by a reference voltage, V_{0Ref} , and the measurement of the output voltage, V_0 where alfa is a gain based on the instrumentation setup. The desired controller, C(s), gives as output the phase difference given by sin δ, such that the error is 0.

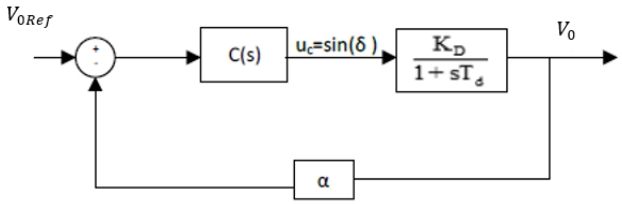

Figure 10-Equivalent control scheme.

To design the controller C(s), it is necessary to establish the relation between the power received from the resonant tank, P_{in} . And the power delivered to the load, P_0. In this expression, it is assumed that there are not any power losses at the converter:

$$P_{in} = P_0 \tag{12}$$

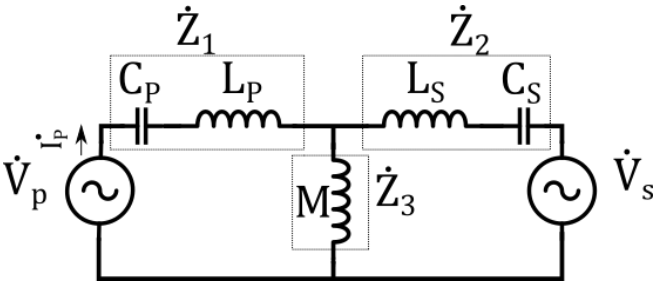

Figure 11-Simplified equivalent circuit of a resonant tank.

To express P_{in} , a simplified equivalent circuit of the resonant tank is illustrated in Figure 11. The voltages source $\dot{V}_p$ and $\dot{V}_s$,which represent the primary and the secondary voltage of the resonant circuit, respectively, can be denoted concerning the phase angle δ as:

$$\dot{V}_p = V_p e^{j0} = V_p \tag{13}$$

$$\dot{V}_s = V_s e^{-j\delta} = V_s \cos\delta - jV_s sin\delta \tag{14}$$

The impedances represented in Figure 11 can be expressed by:

$$\dot{Z}_1 = j\left(X_{L_P} - X_{C_P}\right) = \left(X_{L_P} - X_{C_P}\right)e^{j\frac{\pi}{2}} \tag{15}$$

$$\dot{Z}_2 = j\left(X_{L_S} - X_{C_S}\right) = \left(X_{L_S} - X_{C_S}\right)e^{j\frac{\pi}{2}} \tag{16}$$

$$\dot{Z}_3 = jX_M = X_M e^{j\frac{\pi}{2}} \tag{17}$$

The reactances from the equations (15)(16)(17) of each reactive component can be written as:

$$X_{L_P} = \omega L_P, X_{L_S} = \omega L_S, X_M = \omega M \tag{18}$$

$$X_{C_P} = \frac{1}{\omega C_P}, X_{CS} = \frac{1}{\omega C_S} \tag{19}$$

The current from the primary side $\dot{I}_p$ can also be expressed by:

$$\dot{I}_P = \frac{(Z_M + Z_2)V_p - Z_M V_s e^{-j\frac{\pi}{2}}}{Z_M(Z_1 + Z_2) + Z_1 Z_2} \tag{20}$$
$$= \frac{X_M V_s \sin\delta}{\Gamma} - j\{\frac{X_M V_p - (X_M + (X_{L_P} - X_{C_1}))V_s - X_M V_s \cos\delta}{\Gamma}\}$$

$$\Gamma = X_M\left\{\left(X_{L_P} - X_{C_P}\right) + \left(X_{L_S} - X_{C_S}\right)\right\} + \left(X_{L_P} - X_{C_P}\right)\left(X_{L_S} - X_{C_P}\right) \tag{21}$$

Using the equation (21), it is possible now to arrive at the expression of the active power that is being transferred from the resonant tank to the converter:

$$\begin{aligned} P_{in} &= \mathrm{Re}(\dot{V}_p \dot{I}_p) \\ &= \frac{X_M V_p V_s}{\Gamma}\sin\delta \end{aligned} \tag{22}$$

The expression of the power transferred to the battery, P_0 , can be written only as:

$$P_0 = I_0 V_0 \tag{23}$$

Finally, since $V_p = V_s = V$ it is possible to obtain the following relation:

$$V_0 = \frac{X_M V^2}{\Gamma I_0} \sin\delta \tag{24}$$

Since the controller is dimensioned to have on his output $\sin\delta$, from the equation (24), the gain of the system K_D is:

$$Kd = \frac{X_M V^2}{\Gamma I_0} \tag{25}$$

The control system was implemented using a proportional and integral or PI-control configuration to implement the phase shift. Both gains have different effects on the controller. The proportional gain provides stability and high-frequency response, while the integral gain ensures that the average error reaches zero.. An anti-windup technique was also used to prevent overshoots by the PI-controller's integrator, as illustrated in Figure 12. The PI control function can be expressed as:

$$C(s) = \frac{u_c(s)}{V_{0\mathrm{Re}f}(s) - V_0(s)} = K_p + \frac{K_i}{s} \tag{26}$$

An anti-windup control was also used to prevent overshoots by the PI-controller's integrator, as illustrated in Figure 12.

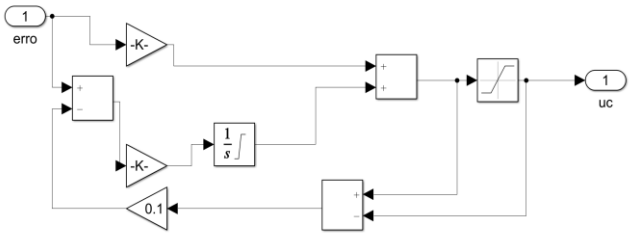

Figure 12-PI controller.

In Figure 12, the closed loop transfer function of the control system is given by:

$$\frac{V_0(s)}{V_{0\mathrm{Re}f}(s)} = \frac{\frac{K_p s + K_i}{s}\frac{K_d}{1+sT_d}}{1+\frac{K_p s + K_i}{s}\frac{K_d}{1+sT_d}\alpha} = \frac{K_d(K_p s + K_i)}{s^2 T_d + s(1+K_d K_p \alpha) + K_d K_i \alpha} = \frac{1}{\alpha}\frac{\frac{\alpha K_d K_i}{T_d}(\frac{K_p}{K_i}s+1)}{s^2 + s\frac{1+K_d K_p \alpha}{T_d} + \frac{K_d K_i \alpha}{T_d}} \tag{27}$$

Comparing the expression (27) to the 2^{nd} order canonical form:

$$G_{2^{nd}}(s) = \frac{\omega_n^{\ 2}}{s^2 + 2\xi\omega_n s + \omega_n^{\ 2}} \tag{28}$$

The proportional gain Kp and integral gain Ki are given by the following expressions:

$$\omega_n^{\ 2} = \frac{K_d Ki\alpha}{T_d} \Rightarrow Ki = \frac{T_d \omega_n^{\ 2}}{K_d \alpha} \tag{29}$$

The expression gives the natural frequency:

$$\omega_n = \frac{(\alpha_z \xi)}{(T_d(2\alpha_z \xi^2 - 1)^2)} \tag{30}$$

where T_d is the statistical delay of the converter given by $T_d = T_{sw}$ and α_z is an adjustable gain. The damping coefficient ξ is equal to $\frac{\sqrt{2}}{2}$ to restrict any oscillations on the output of the controller.

C. Simulation Results

To validate the proposed topology and controller some software tests need to be performed to evaluate if the model is behaving according to what is expected.

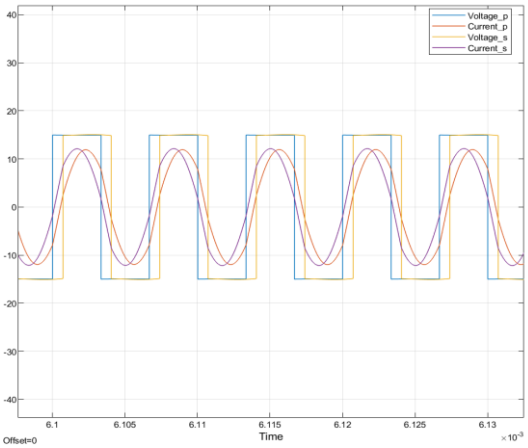

Figure 13-Waveforms on the resonant tank.

The voltage and current waveforms on the resonant tank were measured in the same scope. Figure 13 illustrates the phase-shift between the voltage at the primary and secondary sides of the tank and shows that the currents on each side are in phase with their corresponded voltages, which means the power being transferred is mainly active that one of the main requirements that were intended.

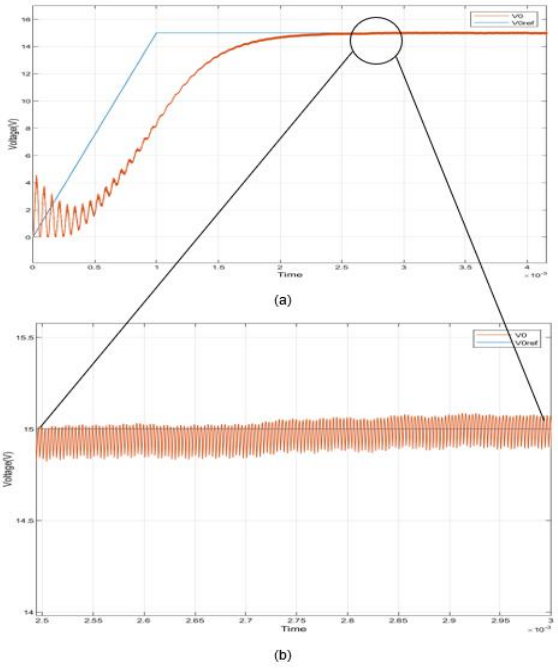

Figure 14-a) Voltage applied to the load,V_0, and reference value of voltage, V_0Ref;b) Zoom between 2 and 3 ms to illustrate the error between the reference and the load voltage.

Regarding the controller,Figure 14 illustrates the error between the load voltage and the reference voltage. It is possible to observe a correct tracking of the reference value with a small voltage ripple around the reference voltage. The error stays near zero until the end of the charging process.

III. Experimental Results

A printed electric board-PCB was designed to control the primary converter and secondary converter of the prototype, one PCB for the primary converter and another PCB for the secondary converter. Since MOSFETs are more adapted to high-frequency applications, both power converters are be implemented using MOSFETs. The complete assembly of both boards can be seen in Figure 15.

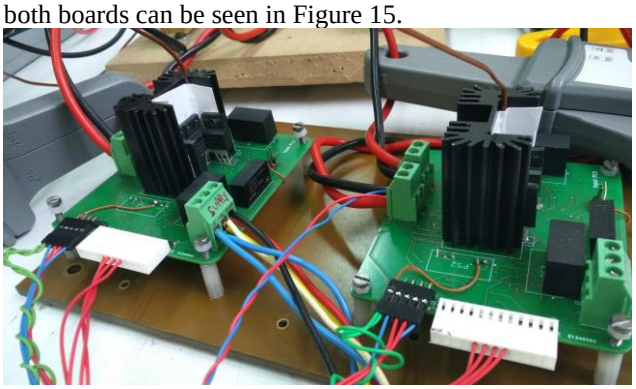

Figure 15-2D view of the PCB.

Some minor modifications were manually made on the board, given a couple of errors made when designing the PCBs regarding the gate drivers' control signals and the capacitors in the DC input entrance. These errors were later corrected, and the PCB schematics were updated.A PWM generator was programmed using a microcontroller. The microcontroller used was the model dsPIC33EV256GMM106 [23] placed on an evaluation board from Microchip [24]. For this specific application, a square wave is generated, switching between a voltage (on) and zero (off). By changing the portion of time that the signal spends on and off usually designated by duty-cycle, which was set to 50 % of the wave period.

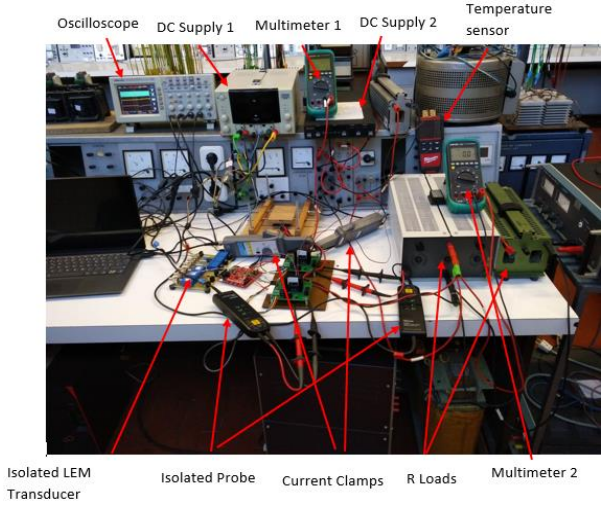

Figure 16-Full Setup for the experiments.

The full setup of the experiment can be seen in Figure 16. This setup uses two DC supplies, one for the power transfer and the other to supply the low voltage to feed all the circuitry in both boards. A temperature sensor was connected to both heatsinks to ensure that temperature limits were not exceeded. There are two currents clamps, one in the input of the resonant tank and the other in the output, to obtain the current waveforms. At the output, two variable resistors were used, in this way, it is possible to adjust the load while doing the tests, and later they were used to test the controller's response to step on the load. A multimeter is used to measure the output voltage and the input voltage, and finally, to control the voltage, an isolated voltage transducer from LEM [25] was used to provide the DC voltage to the microcontroller the closed-loop control could be done.

To find the switching frequency that would lead to the best results, higher and lower frequencies relative to the resonant frequencies were set, tested, and analyzed individually regarding the relation between input and output power and quality of the current waveforms. As illustrated in Figure 17, the frequencies with higher gain in power are between 85 and 98 kHz. The three phases in Figure 17 are the phase shift between the primary and secondary converter. As expected, the highest the phase shift produces the highest the output power, since demonstrated in equation (3), the active power is proportional to the phase shift between the primary voltage and secondary voltage of the resonant tank.

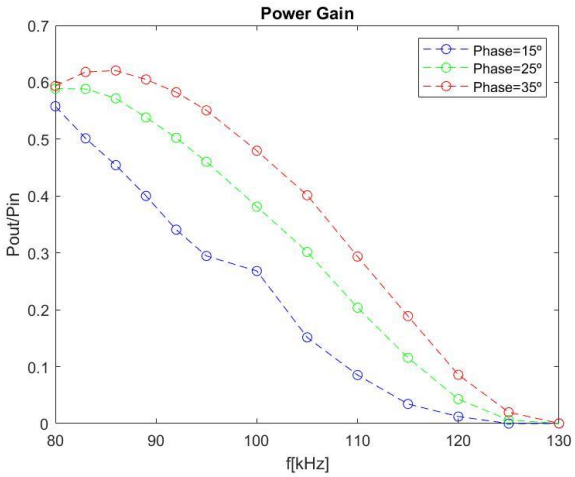

Figure 17-Power Gain for three different phases.

After testing for a set of frequencies between the ranges of 85 to 98 kHz, the frequency of 96 kHz seemed to be the one that produced better waveforms of current in the resonant tank combined with lower noise on the DC output, which is essential when applying the close control loop.

For the frequency of 96 kHz, to serve as another prove that higher phases produce higher output power values, Figure 18 shows the relation between the input and output power plotted against the phase shift between the command signals for the primary converter and the secondary converter. The maximum value of power being delivered to the load is around 75 % of the power being supplied, ranging from the typical nominal efficiencies for wireless chargers [26].

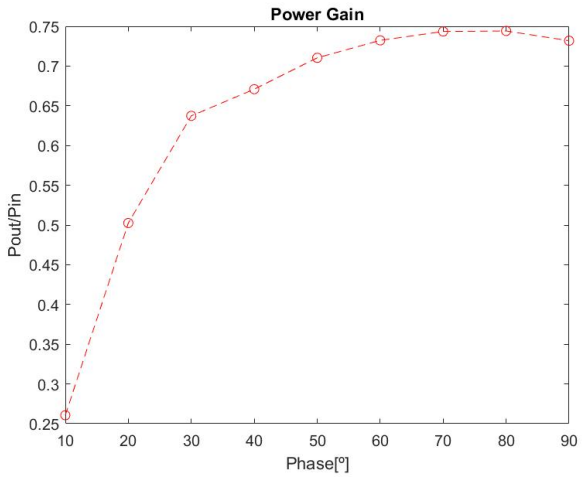

Figure 18-Power gain between phase shifts of 10º to 90º.

Before testing the closed-loop controller, the current and voltage waveforms in the resonant tank can be seen in Figure 19-a) and Figure 19-b). Figure 19-),the voltages were measured at the DC stage of both converters where the controller is phase-shifting the input voltage waveform of the converter and the output voltage of the primary converter.In Figure 19, the voltage measurement at the load stage had some considerable noise, even though this the controller was able to maintain the voltage at the reference value.

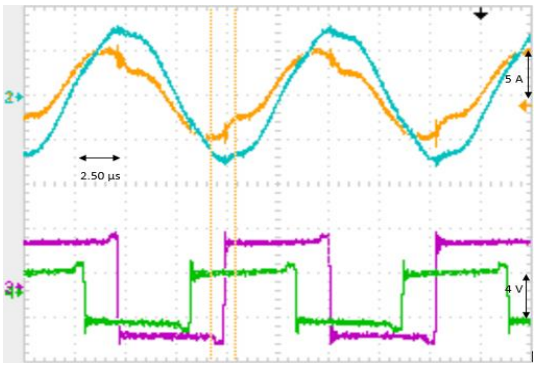

a)

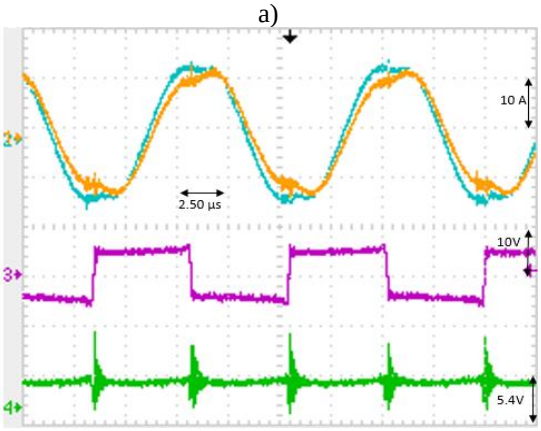

b)

Figure 19- a)-Input current of the resonant tank (orange), Output current of the resonant tank (blue), Input voltage of the secondary converter (purple), Output voltage of the primary converter (green);b)- Input current of the resonant tank (orange), Output current of the resonant tank (blue), Input voltage of the secondary converter (purple), Output voltage at load (green).

The controller was designed to track a reference output voltage. A load was connected in parallel with a manual switch to test the controller's response to an applied step in power. By turning on the switch, a resistive load is placed in parallel with the load stage, causing the output current to increase. The controller must adjust the phase shift between the primary converter and the secondary converter to maintain the load voltage. Figure 20 and Figure 21 illustrate the controller's response to the increase of current when the switch is turned on and the decrease of current when the switch is turn off, respectively. Also, in Figure 22, it is possible to see both transients with an increase of the load current and a decrease of the load current. By looking at Figure 22 , the controller takes proximally 2.50 ms to correct the voltage change at the load, which is considered acceptable since it is close to the controller's time response when designed and tested in the Simulink.

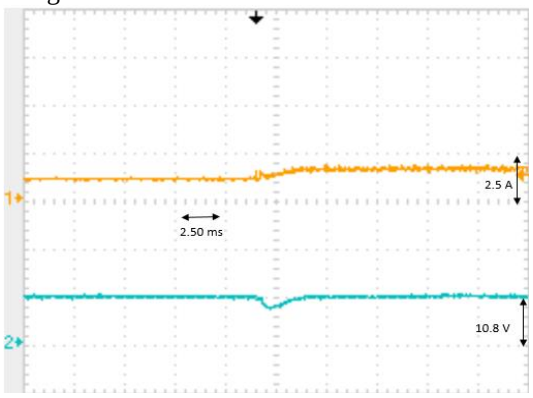

Figure 20-Turn on- Current (Orange);Voltage(Blue).

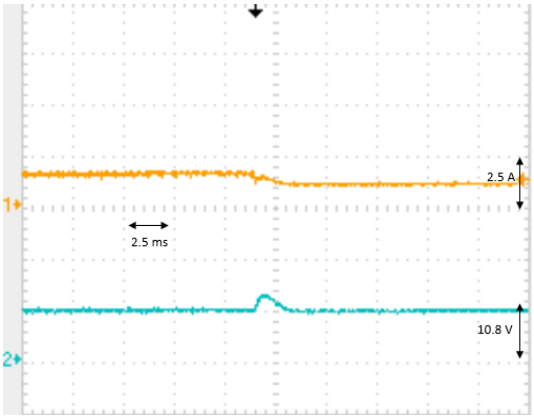

Figure 21-Turn off-Current(Orange);Voltage(Blue).

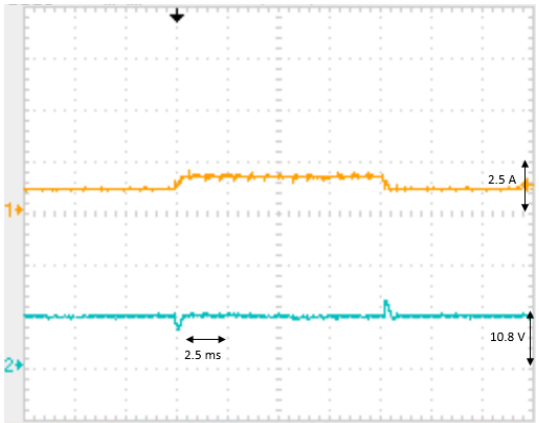

Figure 22-Turn on and off-Current(Orange);Voltage(Blue).

IV. Conclusions

All the research done in this master thesis was aimed to understand better the process of designing and implementing

a wireless inductive charger. After reviewing which current technology of wireless charging seemed, the more promising a prototype was developed. The experiments of the prototype showed a very high sensibility to the operational frequency chosen, in a way that only a specific range of frequencies should be selected to guarantee the highest gain possible of energy transferred, serving as proof of the concept of wireless charging using a resonant tank to enable the power transfer.

Regarding the simulations performed to test the inductive charger, besides controlling the voltage at the load, it would be beneficial to control also the current being supplied to the load in this way fully model of a battery could also be tested, becoming an even more realistic simulation of a wireless charger.

In what concerns the experimental measures, it would also be interesting to analyze the charger's behavior when misalignments and changes of high between the coils are introduced since, in a realistic setting, this usually occurs.

Finally, other possible experiments that should be done for further data collection are experimenting with other compensation topologies such as series-parallel, parallel-series, parallel-parallel, or other more sophisticated combinations to observe the behavior of the charger when switching topologies.

V. References

[1] I.-I. E. Agency, "Global EV Outlook 2020," 2020. [Online].Available:https://www.iea.org/reports/global-ev-outlook-2020.

[2] M. Woodward, D. B. Walton, D. J. Hamilton, G. Alberts, S. Fullerton-Smith, E. Day and J. Ringrow, "Electric vehicles-Setting a course for 2030," *Delloite Insights*, 2020.

[3] S. Abraham, K.Ganesh, A. SenthilKumar and Y. Ducqd, "Impact on Climate Change Due to Transportation Sector – Research Prospective," *Procedia Engineering Volume 38*, pp. 3869-3879, 2012.

[4] W. W. Organization, "Health and sustainable development,"2014.[Online]. Available: https://www.who.int/sustainable-development/transport/health-risks/climate-impacts/en/.

[5] C. E. Regulator, "Market Snapshot: How much CO2 do electric vehicles, hybrids and gasoline vehicles emit?," 2020.[Online].Available:https://www.cer-rec.gc.ca/en/data-analysis/energy-markets/market-snapshots/2018/market-snapshot-how-much-co2-do-electric-vehicles-hybrids-gasoline-vehicles-emit.html.

[6] A. K. Basu, S. Tatiya and S. Bhattacharya, "Overview of Electric Vehicles (EVs) and EV Sensors," in *Sensors for Automotive and Aerospace Applications*, 2019, pp. 107-122.

[7] C. Iclodean, B. Varga, N. Burnete, D. Cimerdean and B. Jurchiș, "Comparison of Different Battery Types for Electric Vehicles," *IOP Conference Series: Materials Science and Engineering 252* , pp. 1-10, 2017.

[8] N.Tesla, "System of Transmission of Electrical Energy," *U.S. Patent 645,576*, 1900.

[9] C. Panchal, S. Stegen and J. Lu, "Review of static and dynamic wireless electric vehicle charging system," *Engineering Science and Technology,Volume 21,Issue 5,Elsevier*, pp. 922-937, 2018.

[10] O. Stielau and G. Covis, "Design of loosely coupled inductive power transfer systems," *Int.Conf. On Power System Technology, PowerCon., 2000, vol 1*, pp. 85-90, 2000.

[11] Z. Liu, H. Zhao, C. Shuai and S. Li, "Analysis and Equivalentof Four-coil and TwoCoil Systems in Wireless Power Transfer," *IEEE PELS Workshop on Emerging Technologies: Wireless Power*, pp. 1-5, 2015.

[12] F. Musavi and W. Eberle, "Overview of wireless power transfer technologies for electric vehicle battery charging," *IET Power Electronics, Volume: 7, Issue: 1, pp.60-66*, 2014.

[13] K.-H. Liu and F. C. Lee., "Zero-voltage switching technique in DC/DC converters," *1986 17th Annual IEEE Power Electronics Specialists Conference*, pp. 58-70, 1986.

[14] N.Mohan and T. a. W.P.Robbins, "Power Eletronics: Converters, Applications, and Design," in *Power Electronics : Converters, Application, and Design, Toronto, Jonh Willey & Sons, INC.*, 1989, pp. 249-295.

[15] Z. Bi, T. Kan, C. C. Mi, Y. Zhang, Z. Zhao and G. A. Keoleian, "Review of wireless power transfer for electric vehicles: Prospects to enhance sustainable mobilit," *Elsevier Volume 17*, pp. 413-425, 2016.

[16] C. Wang, O. Stileau and G. Covic, "Design considerations for a contactless electric vehicle battery charger," *IEEE Transactions on Industrial Electronics. Volume: 52 , Issue: 5, pp.1308–1314*, 2005.

[17] J. Sallán, J. Villa, A. Llombart and J. Sanz, "Optimal Design of ICPT Systems Applied to Electric Vehicle," *IEEE Trans. Ind. Electron.Volume:56,Issue:6, pp.2140–2149*, 2009.

[18] S.Li and C.Mi., "Wireless power transfer for eletric vehicle applications," *IEEE Journal of Emerging and Selected Topics in Power Electronics,Volume: 3 , Issue: 1*, pp. 4-17, 2015.

[19] D. M.Sousa, A.Roque and J. Terras, "Analysis of an inductive charging system for a commercial electric vehicle," *Proceedings of the 2011 14th European Conference on Power Electronics and Applications, EPE 2011*, pp. 1-10, 2011.

[20] M. Simulink, *Version 9.8.0(R2020a)*, Natick, Massachusetts , 2020.

[21] E. Wittenbreder, "Leakage Inductance (Part 1): Friend Or Foe?," HOW2POWER TODAY " Your Power Design Newslette", 2015.

[22] Wurth Elektronik , *(Datasheet)Wireless Charging Coils WE-WPCC Transm Qi 5.8uH 18A 0.012Ohms.*, Revision 001.001, 2017.

[23] Microchip, "(Datasheet)dsPIC33EV 5V CAN-LIN STARTER KIT, 11,"," 2014.

[24] Microchip, "(Datasheet) dsPIC33EV256GM106-5V Robust DSC with CAN, Safety,Motor Control,5,"," 2019.

[25] LEM, "Voltage Transducer LV 25-P," Version 19,2014.

[26] P.Vinciarelli, "Forward Converter Switching at Zero Current," *U.S Patent 4,416,959*, pp. 58-70, 1983.

[27] O. C. G. Stielau, "Design of loosely coupled inductive power transfer systems," *Int.Conf. On Power System Technology, PowerCon., 2000, vol 1*, pp. 85-90, 2000.

[28] G. Ellis, Control System Design Guide:Using Your Computer to Understand and Diagnose Feedback Controllers, Elsevier Inc. 4th edition, 2012.

[29] K. E. Suite, "KiCad Version(5.1.6)," 2020.

[30] C. Panchal, S. Stegen and J. Lu, "Review of static and dynamic wireless electric vehicle charging system," *Engineering Science and Technology,Volume 21,Issue 5,Elsevier*, pp. 922-937, 2018.

[31] Infineon Technologies, "(Datasheet) IRFI4410ZPbF HEXFET® Power MOSFET," REV 2017, 2015.

[32] Infineon Technologies, "(Datasheet)1ED020I12-F2 - Single IGBT Driver IC," REV 2.1, 2017.

[33] A. M. Research, "Global Wireless EV Charging Market," 2020. [Online]. Available: https://www.alliedmarketresearch.com/wireless-electric-vehicle-charging-market.

[34] J. Vázquez and P. R.-S. a. A. P. Torres, "Simulation Model of a 2-kW IPT Charger with Phase-Shift Control: Validation through the Tuning of the Coupling Factor," *Electronics.7.255.10.3390/electronics7100255*, pp. 2-19, 2018.

[35] M. H. Rashid, S. Y. Hui and H. S.-H. Chung, "Resonant and Soft-Switching Converters," *Power Electronics Handbook (Fourth Edition)*, pp. 339-382, 2018.